Proceedings of ASCHT07
1st Asian Symposium on Computational Heat Transfer and Fluid Flow
October 18-21, 2007, Xi'an, CHINA

Paper No. ASCHT2007-002

NUMERICAL STUDY ON FLUID FLOW CHARACTERISTICS OF PERISTALTIC PUMP

K. Tatsumi, Y. Matsunaga[§], Y. Miwa and K. Nakabe*
Department of Mechanical Engineering and Science, Kyoto University, Kyoto 606-8501, Japan
§ Denso corporation, Kariya, Aichi 448-8661, Japan
*nakabe@me.kyoto-u.ac.jp

ABSTRACT

Fluid flow characteristics in a peristaltic micro pump, which can be applied to Lab-on-a-Chip or Micro Total Analysis Systems (μ-TAS), were numerically investigated. For the present computational analysis, we assumed a simple sinusoidal wave pattern to simulate the peristaltic motion of flexible channel wall and applied the immersed boundary (IB) method to the treatment of the wall boundary. The effects of the parameters of the peristaltic motion such as the amplitude and velocity of the sine wave upon the flow characteristics and pump performance were evaluated in the present paper. The shapes of the wall motion were also changed from the sinusoidal pattern to saw-toothed or trapezoidal patterns to examine the potentiality of the pumping flow rate increase.

INTRODUCTION

The length scale of micro fluidic devices in the systems of μ-TAS or power-MEMS is in the range of order 1 ~ 100μm, accompanied by a large decrease of the flow Reynolds number. Then, fluid flows in the channels of such devices become laminar and hardly mix in comparison to turbulent mixing [1 ~ 3]. Figure 1 shows a schematic illustration of micro fluidic device which is composed of micro pumps, mixers and sensors. The authors' research group has investigated the enhancement of mixing using ribs, trenches and jet flows through some branch channels for designing effective micro mixers [4] and also produced micrometer-scale thermo-sensitive films for the development of micro temperature sensors [5]. In the present article, the authors paid attention to micro pumps aiming at the development to effectively feed fluids to the micro fluid devices.

Peristaltic pumps are regarded as one of the promising types of micro pumps for fluid-MEMS of μ-TAS. In Ref. [6], a proto-type peristaltic pump was manufactured and experimentally examined. The active part consisted of piezoelectric (PZT) elements was attached to a micrometer-scale flexible channel wall from the outside, which is schematically illustrated in Fig. 2. Fluids can be transported through the channel from the left side to the right side, in response to the peristaltic motion of the channel wall. This mechanism can simplify the structure of the pump device. As a more convenient feature, this pump makes it available for multiple medical diagnoses to only replace disposable test-section channels but not the pump itself, resulting in cost and time reductions.

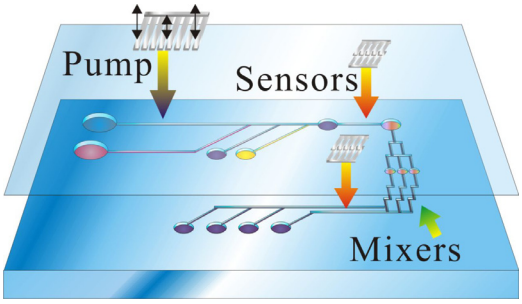

Fig. 1 Schematic illustration of μ-TAS.

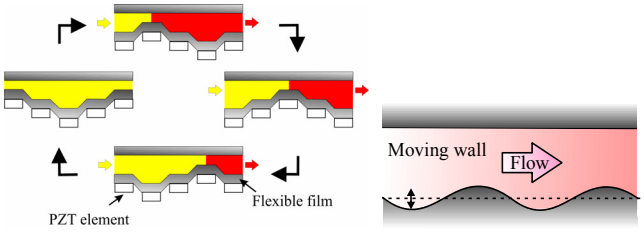

Fig. 2 Schematic view of peristaltic micro-pump driving.

In order to design this type of the pump with emphasis on an effectively-controlled fluid transportation, the flow characteristics in the channel are investigated with

computational method, and the effects of the geometrical parameters such as the amplitude and velocity of the peristaltic motion of the wall on the pump performance was examined. The effect of the moving wall patterns are also discussed in the present study.

NUMERICAL PROCEDURES

The governing equations solved in the computational domain shown in Fig. 3 were two-dimensional, time-dependent and incompressible continuity and Navier-Stokes (N-S) equations:

$$\frac{\partial U_i}{\partial x_i} = 0 \quad (i = 1,2)$$

$$\rho \frac{DU_i}{Dt} = -\frac{\partial P}{\partial x_i} + \frac{\partial}{\partial x_j}\left(\mu \frac{\partial U_i}{\partial x_j}\right) \quad (i = 1,2)$$

where U_i is the velocity of the Cartesian x_i direction. ρ and μ are the fluid density and viscosity, respectively. The working fluid was water as a Newtonian fluid.

A simple sinusoidal wave pattern was assumed to simulate the peristaltic motion of the channel wall, which can be represented using the IB method [7, 8] adopted in the finite-volume computational code. Following the IB method, virtual body forces f_i^τ expressed below can be added to the N-S equation at every computational time step τ and at suitable grid locations to adjust the fluid velocities to the wall speeds corresponding to the peristaltic motion:

$$f_i^\tau = \rho \frac{U_{IB,i}^\tau - U_i^{\tau-\Delta\tau}}{\Delta\tau} + \rho \frac{\partial}{\partial x_j}\left(U_j^\tau U_i^\tau\right) + \frac{\partial P^\tau}{\partial x_i} - \frac{\partial}{\partial x_j}\left\{\mu\left(\frac{\partial U_i^\tau}{\partial x_j} + \frac{\partial U_j^\tau}{\partial x_i}\right)\right\}$$

where $\Delta\tau$ denotes the computational time interval. $U_{IB,i}{}^\tau$, U_i^τ and P^τ represent the target velocity for IB method, the fluid velocity in the IB-represented boundary region and the corresponding pressure, respectively. Fluid velocities on the grids closest to the wall region are estimated with linear-interpolation of area-weighted average velocities against the distance from the wall surface along a normal line to the surface.

In the preliminary computation, flow velocity distributions of flows in a bent channel or flows over a backward-facing step were computed. The predicted reattachment length in the case of the backward-facing step flows showed a good agreement with other researchers' data, the figure of which is omitted on account of limited space in the present paper.

The computational domain and coordinate system for the channel in the peristaltic pump are shown in Fig. 3. The channel height, H, and the streamwise wavelength, L, were fixed at a constant value as H = 100μm and L/H = 10, respectively. These parameters including other geometric parameters, the bottom wall amplitude A_1 (the top wall one A_2, also) and the wall speed c, are tabulated in Table 1 with their case labels.

The cases categorized in Table 1 were some representative cases examined in the present study. Θ denotes a phase difference between the top and bottom walls, in the cases A05c01b and A05c01c of which both the top and bottom walls simultaneously move with the sinusoidal amplitude halved as compared to the other cases. The last two cases labeled as A1c01s and A1c01t in Table 1 represent, respectively, sawtooth and trapezoidal patterns of the wall motion. These four cases will be argued with more details in a later section.

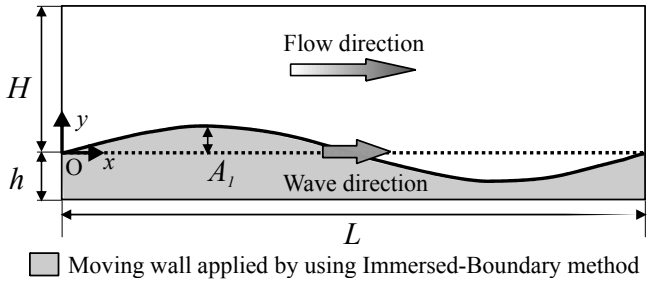

Fig. 3 Computational domain.

Table 1 Geometric parameters.

Label	A_1/H	A_2/H	c [m/s]	Grid	Θ [rad]
A1c01	0.1	0	0.1	200×140	—
A1c1	0.1	0	1.0		
A1c10	0.1	0	10		
A05c01b	0.05	0.05	0.1	200×220	0
A05c01c	0.05	0.05	0.1		–π
A1c01s	0.1	0	0.1	200×140	—
A1c01t	0.1	0	0.1	300×140	—

RESULTS AND DISCUSSION

Cases of one-side sinusoidal wall motion

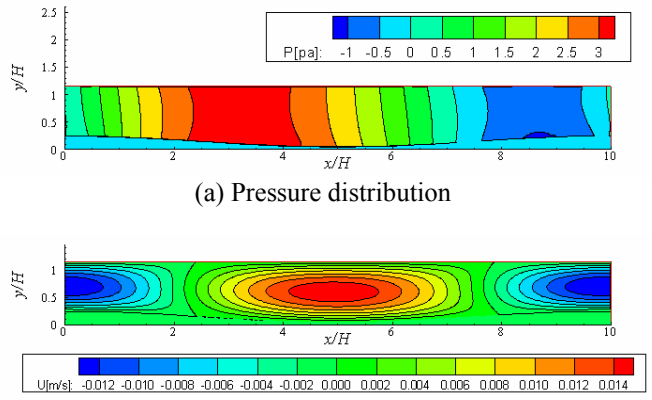

(a) Pressure distribution

(b) Streamwise velocity distribution

Fig. 4 Instantaneous contours of pressure and streamwise velocity (Case A1c01).

Figure 4 (a) and (b) shows typical results of instantaneous fluid pressure and streamwise velocity contours. At this instance, the region of $2 < x/H < 4$ retains higher pressures above the surrounding pressure, where coincides with the negative-gradient slope region of the wall forming a sinusoidal traveling wave from the left side to the right side. Relatively lower pressure regions are located in the front and in the rear of

the higher pressure region. Putting the pressure contours and the velocity contours for comparison, it is noticed that the regions of positive and negative streamwise velocities exist respectively downstream and upstream of the higher pressure region. Also, as shown in Fig. 4 (b), the positive maximum of forward-directional velocity is found to be a bit larger than the negative maximum of backward-directional velocity, which implies that the net transportation of the working fluid occurs as the time passes by, during one cycle.

Figure 5 (a) shows the path lines of one cycle in the case of A1c01, starting from three different spanwise positions (x/H, y/H) = (5, 0.1), (5, 0.4) and (5, 0.8), while Fig. 5 (b) shows the path lines analytically predicted by Yin and Fung [9]. What is apparently obvious on comparing both figures (a) and (b) is that the patterns of the path lines are similar to each other. The fluid moves forward almost in the first half of one cycle and then backward in the latter half, corresponding to the wall motion. These fluid motions produce a pulsating flow with a net flow rate during one cycle.

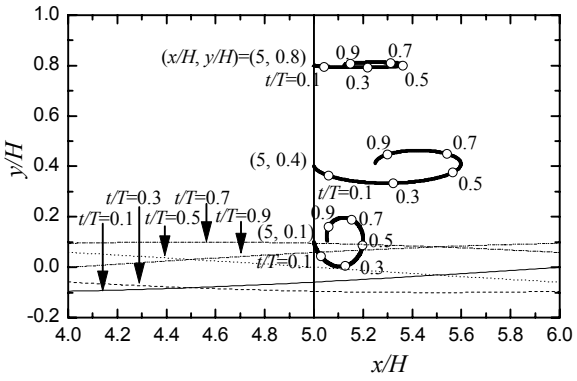

(a) Present results (Case A1c01)

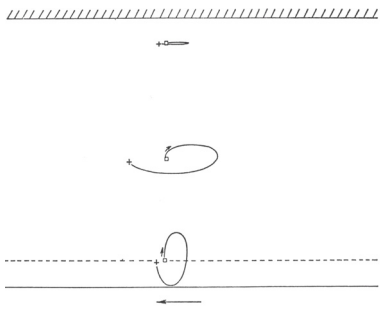

(b) Results of Ref. [9]

Fig. 5 Comparison of the numerically-obtained path lines to other researchers' data.

Figure 6 (a) and (b) shows how the amplitude, A, and velocity, c, of the moving wall have influences on the time-averaged streamwise fluid velocity, U_m. The ratio of U_m to the moving wall speed, c, was assigned to the scale of the ordinate. As shown in Fig. 6 (a), the relation between U_m/c and A/H shows a good agreement with the fitting function of a parabolic curve. This trend also coincides with the analytically-obtained results shown in Ref. [9]. In Fig. 6 (b), U_m/c keeps constant in relatively lower wall speed range, c = 0.01 ~ 0.1m/s. As the wall speed is increased to c = 1.0 and 1.5m/s, U_m/c is gradually decreased, which implies that U_m is not linearly increased with the wall moving speed, c.

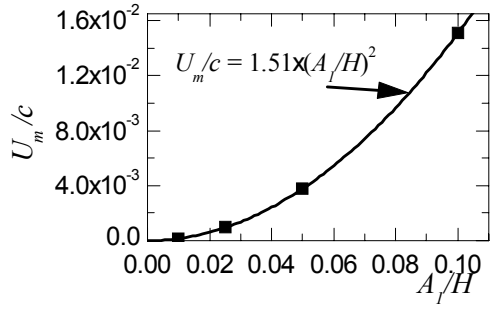

(a) Effect of A_1/H

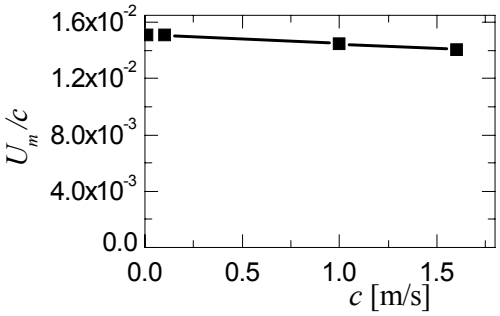

(b) Effect of c

Fig. 6 Relations among U_m/c, A_1/H and c.

To understand this non-linear trend of the bulk fluid velocity against the relatively higher wall moving speed, phase-averaged velocity distributions were calculated. Figure 7 (a) and (b) shows the spanwise distributions of streamwise velocity, U, at the location of x/H = 5 in the two cases of A1c01 and A1c1. $\hat{t}/T$ represents the dimensionless time, i.e., the ratio of phase-averaged time to a time-period of one cycle. In the relatively-low wall speed case of (a) A1c01, the velocity changes its sign periodically in one cycle, and the velocity distributions maintain almost parabolic patterns. In the higher wall speed case of (b) A1c1, on the other hand, the velocity distribution pattern deforms from a parabolic shape to a quartic-like shape possessing a depression around the channel center.

This deformation of Case A1c1 is considered to be attributable to a phase difference between the motions of the fluid core and the fluids adjacent to both the top stationary wall and bottom moving wall. As clearly seen in the velocity distribution of Fig. 7 (b), the fluids in the vicinity of the both walls at $\hat{t}/T$ = 0.3 can act in accordance with the bottom wall motion, while the fluids around the channel center do not obediently follow the wall motion. At $\hat{t}/T$ = 0.7, the fluids in the vicinity of the wall already have positive velocities while the fluid core has still negative velocities, the fact of which suggests the occurrence of the phase difference and may cause

the aforementioned non-linear relation between the bulk fluid velocity and the wall speed.

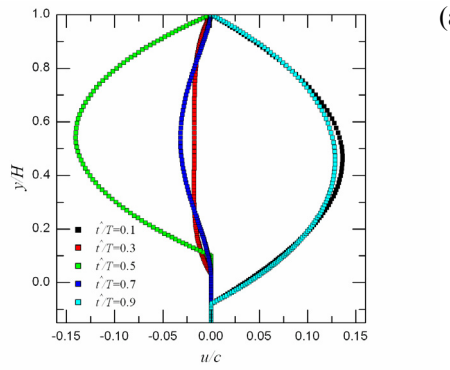

(a) Case A1c01

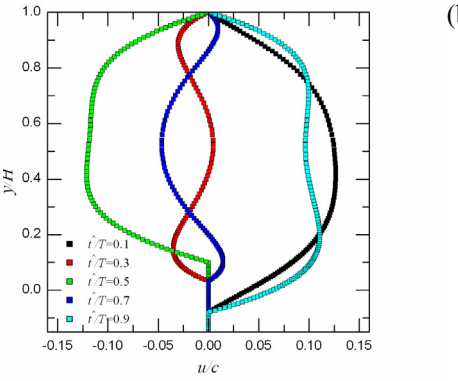

(b) Case A1c1

Fig. 7 u/c distributions at $x/H = 5.0$.

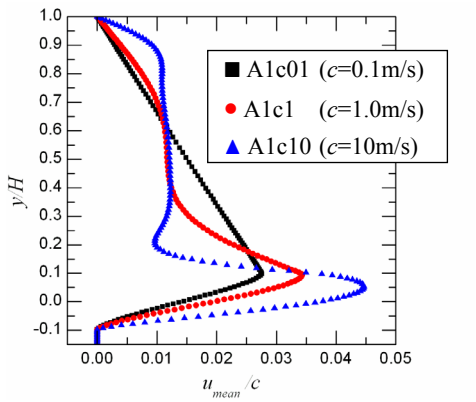

Fig. 8 Time-averaged streamwise velocity distributions.

Time-averaged streamwise velocity distributions along the spanwise direction are shown in Fig. 8. In the case of A1c01, the maximum streamwise fluid flow velocity is found to be located at y/H ~ 0.1. As the moving speed of the wall is increased, the velocities near-wall regions are correspondingly increased. The velocity distributions in the fluid core region, however, show the opposite trend that the fluid velocity is decreased with an increase in the wall speed. Thus, it will be almost impossible to increase the net flow rate linearly by increasing the wall speed, because of the cancellation superimposed between the velocity decrease in the core region and the velocity increase in the near-wall region.

Cases of other wall motion patterns

In the previous section, the flow characteristics of the fluid driven by the one-side sinusoidal wall motion were clearly reveals through the present numerical simulation using IB method. In this section, some other different wall motion patterns were numerically simulated to examine how the flow patterns or the net flow rates change.

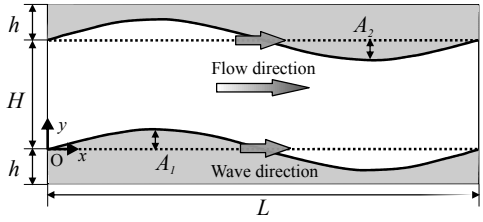

(a) Sinusoidal wall on both sides (Case A05c01b, $\Theta = 0$)

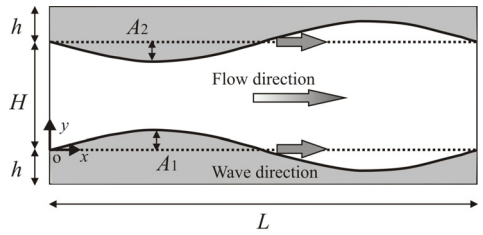

(b) Sinusoidal wall on both sides (Case A05c01c, $\Theta = -\pi$)

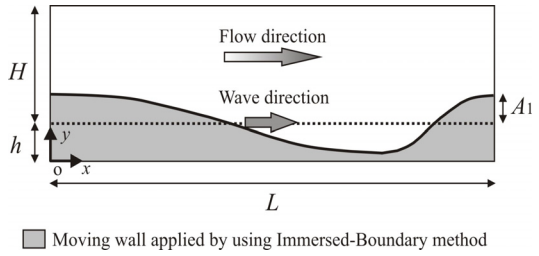

(c) Sawtooth-shape wall (Case A1c01s)

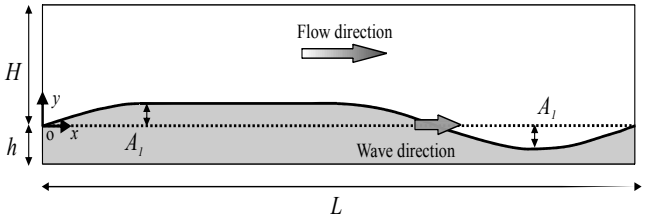

(d) Trapezoidal-shape wall (Case A1c01t)

Fig. 9 Computational domains of other wall moving patterns.

There are three types of motion pattern adopted here: the first one is the type of sinusoidal-shape on both top and bottom walls, the second one sawtooth-shape and the last one trapezoidal-shape, which are shown in Fig. 9 (a) ~ (d). Geometric parameters were summarized previously in Table 1. The total amplitude of both the top and bottom walls in the

cases of (a) A05c01b and (b) A05c01c is equal to the amplitude of the one-side wall motion case, i.e. the reference case, A1c01. Only a difference of the computational condition between these two cases of A05c01b and A05c01c is the parameter of a phase difference, Θ ; zero (no delay) or -π (half-cycle delay). The sawtooth-shape of (c) A1c01s was described using the combination of two different wave-length sinusoidal waves as follows:

$$y = A\sin\left(\frac{2}{3}\frac{2\pi}{L}(ct-x)+\theta_{t=0}\right) \quad \left(0 \le x/L \le \frac{3}{4}\right)$$
$$y = A\sin\left(2\frac{2\pi}{L}(ct-x)+\theta_{t=0}\right) \quad \left(\frac{3}{4} \le x/L \le 1\right)$$

The trapezoidal-shape of (d) A1c01t was composed with a sinusoidal wave and a rectangular wave.

The effects of the above-mentioned patterns of the wall motion on the time-averaged streamwise velocity are summarized in Table 2. The time-averaged streamwise velocity U_m/c in the case of the wall motion on both sides with the half amplitude and the same phase (Case A05c01b) is found to be extraordinarily small by the order of 3, compared to the reference case, A1c01, which indicates that almost no fluid transportation occurs in the channel. In the case of the half-period phase shift (Case A05c01c) with the half amplitude, no increase of U_m/c was obtained, compared to the reference case, A1c01. Even if the wall motion changes from the sinusoidal pattern to the sawtooth pattern (Case A1c01s), no increase of U_m/c was obtained, also. The case of the combined trapezoidal-sinusoidal wall motion pattern (Case A1c01t) was found to achieve 6% increase of U_m/c, compared to the reference case, A1c01.

Table 2 Wall shape effect on U_m/c.

Label	A1c01	A05c01b	A05c01c
	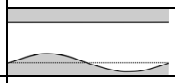	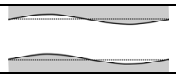	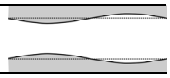
U_m/c	1.51×10^{-2}	1.67×10^{-5}	1.51×10^{-2}

Label	A1c01s (Sawtooth)	A1c01t (Trapezoid)
U_m/c	1.51×10^{-2}	1.60×10^{-2}

Lastly, the mechanical work given to the fluid by the peristaltic movement of the pump itself during one cycle will be evaluated using the following equation.

$$W = \frac{\int_0^L \int_0^{\Delta T} (P_w(x,t) + \tau_{w,y}) V_w(x,t) dt dx}{L\Delta T}$$

where ΔT is a time period of one cycle. P_w, V_w and $\tau_{w,y}$ indicate, respectively, a fluid pressure, a y-component fluid velocity and y-component shear stress on the wall surface.

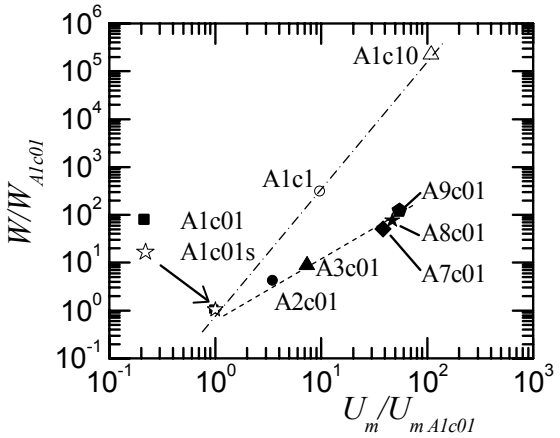

Fig. 10 Mechanical work, W vs. U_m.

The relation between the evaluated mechanical work per unit area and the time-averaged streamwise velocity is shown in Figure 10. The scales of both coordinate axes are normalized, based on the reference case, A1c01. With respect to the wall motion speed c (Cases A1c01, A1c1 and A1c10), both U_m and W are increased as plotted with a chain line. In case that another set of computational condition was executed by changing the wave amplitude, A/H = 0.1 ~ 0.9 under the wall speed kept constant at c = 0.1m/s (Cases A1c01 ~ A9c01), a similar trend of the increases concerning both U_m and W was obtained as plotted with a broken line. In comparison with these two lines, the gradient of the chain line is larger than the one of the broken line. This implies that the peristaltic pump requires more external energy to obtain the same flow rate by the wave speed increase than by the wave amplitude increase.

In the case of sawtooth-shape pattern, there is no apparent difference of both U_m and W from the reference case A1c01. 3% increase of W in the case of A1c01s was found with careful inspection, compared to the reference case A1c01. This indicates that the pump efficiency is influenced more significantly by the wave amplitude and speed than by the wall shape pattern.

CONCLUSIONS

The characteristics of fluid flows in a peristaltic micro pump were numerically investigated. A simple sinusoidal wave pattern was assumed to simulate the peristaltic motion of flexible channel wall. Some other different wave patterns were also adopted in the present numerical simulation. The effects of the amplitude and speed of peristaltic wave upon the flow characteristics and pump performance were summarized as follows:

1. The fluid moves back and forth and produces a net flow rate in one cycle of the peristaltic pump motion.
2. The relation between time-averaged streamwise velocity (bulk velocity) and wave amplitude can be expressed by a quadratic equation in relatively smaller wave amplitudes.
3. Non-linear trend of the bulk velocity against the wall moving speed can be cause by a phase difference between

the motions of the fluid core and the fluid adjacent to the walls.

4. No remarkable increase of the bulk velocity is obtained even if the wave shape pattern is changed.
5. The pump efficiency is influenced more significantly by the wave amplitude and speed than by the wall shape pattern.

Further investigations will be reported somewhere soon on the flow and also heat transfer characteristics in detail for various motion patterns of the peristaltic pump.

ACKNOWLEDGMENTS

This study was carried out as a part of Advancing Technology Excellence 'Nano-Medicine' project, which is under Kyoto City Collaboration of Regional Entities assigned by JST.

REFERENCES

[1]G.E. Karniadakis and A.Beskok, Micro Flows – Fundamentals and Simulation, Springer.,2002.

[2] E.Wolfgang, H.Volker and Holger Löwe, Microreactors, Wiley-VCH.,2000

[3]N.T. Nguyen, and S.T.Wereley,Fundamentals and Applications of Microfluidics, Artech House,2002.

[4] K.Tatsumi, Y.Tsukanaka, and K.Nakabe, Groove-Patterns Effects on Mixing Performance in a Micro-Mixer, Proc.17th Int'l Symp. on Transfport Phenomena, CD-ROM (No. 2-B-I-1),2006.

[5] T. Jida, K. Tatsumi, and K. Nakabe, Measurements of Fluid Temperature in Microchannels Using Embedded-Membrane-Sensors Proc. 82th JSME-Kansai Spring Meeting, 4-1:2-1,2007. (in Japanese).

[6] I. Kanno, T. Suzuki, H. Hata , H. Shintaku, S. Kawano, and H. Kotera, Development and Characterization of a Traveling Wave Micropump Driven by Piezoelectric Actuators. 2nd Int'l Symp. Micro & Nano Technology (ISMNT-2),pp:226 – 229,2006.

[7] C. S. Peskin, Numerical Analysis of Blood Flow in the Heart J.Computational Physics,25:220 – 252,1977.

[8] M.C. Lai, and C. S. Peskin,An Immersed Boundary Method with Formal Second-Order Accuracy and Reduced Numerical Viscosity J.Computational Physics, 160:705-719, 1977.

[9] F.C.P.Yin, and Y.C.Fung, Comparison of Theory and Experiment in Peristaltic Transport J. Fluid Mechanics, 47 : 93–112,1971.